High throughput laser-induced fluorescence droplet micro-thermometry

Gautier Guérin, Abdel El Abed

▶ **To cite this version:**

Gautier Guérin, Abdel El Abed. High throughput laser-induced fluorescence droplet micro-thermometry. International Journal of Heat and Mass Transfer, 2023, 212, 10.1016/j.ijheatmasstransfer.2023.124230 . hal-04424673

HAL Id: hal-04424673
https://hal.science/hal-04424673

Submitted on 1 Apr 2024

HAL is a multi-disciplinary open access archive for the deposit and dissemination of scientific research documents, whether they are published or not. The documents may come from teaching and research institutions in France or abroad, or from public or private research centers.

L'archive ouverte pluridisciplinaire **HAL**, est destinée au dépôt et à la diffusion de documents scientifiques de niveau recherche, publiés ou non, émanant des établissements d'enseignement et de recherche français ou étrangers, des laboratoires publics ou privés.

High throughput Laser-Induced Fluorescence Droplet Micro-thermometry.

Gautier Guérin[a], Abdel El Abed[a,*]

[a]*Laboratoire Lumière Matière et Interfaces (LuMIn), Institut d'Alembert, Ecole Normale Supérieure Paris Saclay, CentraleSupélec, CNRS, Université Paris-Saclay, 4 avenue des Sciences, Gif-sur-Yvette, 91190, Essonne, France*

Abstract

This paper assesses a new temperature measurement method at the microscale at high throughput. This non-invasive method is based on laser-induced fluorescence of highly monodisperse dye-doped flowing microdroplets in microfluidic channels. Laser-Induced-Fluorescence (LIF) of two thermo-responsive dyes (Rhodamine B and rhodamine 110) enables temperature sensing in real-time at high acquisition rates. A single excitation with a 532 nm laser shows satisfying fluorescent emission with no absorption overlap. The emission signals from both dyes are analyzed, and the ratio of both fluorescence intensities shows a -1.4% variation per degree, similar to our observations with dissolved dyes in a single phase microfluidic flow. The ratiometric computational method gives similar results for two droplet sizes, underlining the method's versatility for various microchannel sizes. The thermal evolution of microdroplets' inner temperature is evaluated throughout a cooling of the microfluidic chip, allowing the study of heat exchanges at the droplet microscale.

Keywords: Droplet Microfluidics, Laser Induced Fluorescence, Thermal measurements, Lab-On-Chip

1. Introduction

Lab-on-chip technology aims to improve a variety of testing apparatuses through system miniaturization. From antibody detection for disease diag-

*Corresponding author
Email address: abdel.el-abed@ens-paris-saclay.fr (Abdel El Abed)

nosis to the determination of pollutants concentration in bulk, micro-scale total analysis systems (μTAS) proved their relevance and potential in many scientific fields [1, 2, 3, 4]. But for successful implementation at the microscale, thorough control of physicochemical parameters within the microfluidic chip is frequently required. In particular, temperature measurement within microscale flows can quickly become challenging as few techniques allow for both non-invasive and local measurements in fluids. Yet it is often a key parameter that needs to be accounted for in most reactions or physical mechanisms. This is especially true in droplet technology where the analyte is separated within thousands of droplets, flowing through a continuous phase of different nature. This technology relies on the production and manipulation of highly monodisperse microdroplets of fluids, with a high degree of control and reproducibility [5]. Droplets can be formed, filled with reagents, and manipulated at kilohertz rates. These droplets, usually picoliter-sized, are held together by surface tension and offer a unique confined environment particularly suited for process analysis [6]. High-rate methods of temperature determination within droplets are therefore needed for the high-scale study of chemical reactions in numerous droplets. The droplets' distinctive characteristics both in terms of production high rate and small size thus call for new measurement techniques.

In this paper, we propose a method to determine the droplets' temperature via fluorescent measurements. By using adequate fluorescent dyes with temperature-sensitive quantum yields, we can determine the inner temperature through volumetric illumination by a single-wavelength continuous laser. This method referred to in the literature as two dyes, one color laser-induced fluorescence (2d/1c LIF) is particularly well-suited for droplet fluorescence measurements. Ratiometric comparison of our dyes' fluorescence intensities allows us to circumvent variations of droplet volume or laser illumination throughout experimentation.

For this study, we exploit the fluorescence temperature dependence of Rhodamine B and Rhodamine 110. On one hand, Rhodamine B's quantum yield decreases with temperature (-2.3%/°C in water [7]). This behavior is well-documented and is owed to the thermal mobility of its conjugated diethylamino group, impacting the photon conversion mechanism [8, 9]. With a broad and thermally stable absorption peak, excitation can be performed with a great range of wavelengths (usually between 488 nm and 550 nm), while excitation can be filtered with a lowpass filter (>550nm). On the other hand, Rhodamine 110 presents very little quantum yield variation

(+0.13%/°C in water [7]) and is therefore broadly used as a normalization component thanks to its low bandwidth overlap with RhB's absorption. Usually, the excitation of the Rh110 dye combination is performed at 488 nm where both dyes have relevant absorption, but this combination was also reported for excitation with a 532 nm laser [10]. In this case, however, emission from the Rh110 dye is greatly hindered by the excitation filtering. The resulting emission signal is eventually underestimated, as nearly half of the peak emission is ultimately filtered. Despite that, variation of Rh110 are still measurable, and its evaluation resulted in a greater increase than reported through the QY (+0.4%/°C > +0.13%/°C). Indeed unlike its counterpart, Rh110 shows an absorption shift toward longer wavelengths with increasing temperature. This phenomenon has been thoroughly described by Chaze et al [11] for fluorescein and Rhodamine 560 (generic name of Rhodamine 110). While this absorption shift was not reported for excitation at 488 nm (less than 0.05%/K at 488nm [7]), for a 532nm excitation this phenomenon is responsible for the increased emission variation (as reported in [10, 12]). Rhodamine B and 110's emission hence behave with opposite trends. This was experimentally confirmed with the acquisition of emission spectra at various temperatures. With this method, we manage to access the droplet temperature with a fairly simple apparatus in a highly reproducible way.

2. Material and methods

2.1. Design and microfabrication

The microfluidic chip was produced following a soft lithography procedure previously described in ref. [2]. It revolves around the transfer of a pre-defined pattern from a mask onto a photoresist epoxy layer (SU-8 resin deposited onto a silica wafer) through UV illumination. The illumination parameters (power, exposition time), along with the intrinsic properties of chosen epoxy will define the etching depth, which corresponds to the final microfluidic channels height. For our experiments, the channel depth was set to 50μm. Once developed, a mix of PolyDiMethylSiloxane (PDMS) and its crosslinking agent is cast onto the pattern, degassed in a vacuum chamber for 45 min, and then heated at 75 °C for 2h. The polymerized silicone is then cautiously uncasted, cut, punched, and plasma-cleaned to allow adhesion and sealing of the pattern onto a 1mm thick borosilicate glass slide. The microfluidic channels are subsequently rendered fluorophilic by another plasma cleaning step followed by injection through the channel of a 5% solution of

TriChloro-perfluoro-octyl silane in HFE7100 (Inventec). After rinsing, we proceed with the last drying step (1h at 75 °C) before the final use of the chip. Silanization improves the continuous phase wetting of the channel and therefore enhances droplet quality (size dispersion & frequency).

2.2. Droplet generation

The droplet production is carried within a dedicated chip with a design similar to ref.[2, 13]. Dual syringe pumps (NEMESYS, Cetoni Gmbh) and PTFE tubings allow stable flow rate injection of the two fluids in the microfluidic system. The microchannel design consists of a so-called "flow focusing" geometry allowing passive shearing of aqueous phase by fluorinated oil flow through a tailored nozzle. For the continuous phase, a high molecular weight fluorinated oil (HFE 7500, 3M Novec) mixed with a PEG-PFPE type commercial surfactant dSurf® (Fluigent) was used. A surfactant concentration of 1%vol allows satisfying stability of the aqueous droplets. The aqueous phase is composed of methanol and deionized water (80/20 ratio in volume) in which were dissolved fluorescent dyes. Rhodamine B and Rhodamine 110 are added to the mixture to reach 10 μM concentration for each dye. The Rhodamines' equal concentrations simplifies the ratio-metric computation making concentration ratio equal to unity. HFE 7500 and an 80/20 binary solution of methanol/water makes a convenient choice as Rhodamine's QY increases inversely with the solvents polarity [14]. The presence of deionized water at 20%vol is necessary for droplet formation and stability against coalescence. The d-Surf surfactant used in this study is indeed designed for water/fluorocarbon emulsions stabilization The produced droplets show very limited coalescence and high monodispersity (<1% size variation at a given temperature). Two chips with different nozzle sizes ensured steady production of $\varnothing$ 55 μm and $\varnothing$ 35 μm droplet population at various continuous (Qc) and dispersed (Qd) flow rates (Qc=300 μL/h; Qd=50 μL/h and Qc=150 μL/h; Qd=20 μL/h respectively).

2.3. Fluorescence detection and temperature variation

As the microfluidic chip is made of transparent medium (PDMS and glass) the fluorescent detection of dyed droplets could be performed with an inverted microscope. The excitation is performed through the manual focusing of a 532 nm continuous laser beam adjusted onto the channel flow (laser diode, CNI MGL-W 532 nm) to reach maximal emission. With an x50 standard objective, the resulting focusing point reaches 5 μm in diameter which

is significantly smaller than our droplets ($\varnothing$[35 - 55]μm). The fluorescence signal picked up by the microscope objective is collected by a parabolic mirror. This mirror sends the signal back onto a dichroic mirror followed by two sets of filters and photo-multiplicator tubes (HAMAMATSU H10721 series), one for each emission wavelength (see fig.2 for details). Illumination was performed 1mm away from the nozzle, down the flow to reach the droplet's stabilization. A microscope-staged incubator (TOKAI HIT NI-F1) is used to maintain the system at a set point temperature. The 532nm wavelength is convenient for Rhodamine B (RhB) excitation as its absorption peak approaches 546 nm in methanol. This is though unconventional for Rhodamine 110 (Rh110) as it shows low absorption at this wavelength (see fig.1). Still, emission from both dyes can be detected with a satisfying Signal-to-Noise Ratio (SNR>10) and the wavelength separation can be performed with a high-pass filter (λ_{max}=520nm) and a low-pass (λ_{min}=550 nm). With such filters, the overlap between both emissions is ignored, at the cost of an underestimation of each peak area. Absorption and emission spectra of the dyes mix (corresponding to the blue dotted line on fig. 1) show limited interaction: in the mixed sample, Rh110's emission (525nm) is not significantly affected by the RhB broad absorption band (from 480 to 580 nm). Re-absorption of Rh110's fluorescence by RhB in bulk is therefore neglected. It is also considered that the re-absorption effect is even less likely to occur at a small scale, where absorption is reduced (absorption decreases exponentially with the optical path) and where the isotropic nature of fluorescence emission is favored by the increased surface-to-volume ratio (fluorophores near the phase interface undergo less re-absorption). The repeatability of the measurement protocol is insured by the application of the same script to all sets of measurements. The variation of the emission intensity over the temperature can be explained by two different mechanisms. Considering the optical pumping of a diluted fluorescent molecule without saturation, its fluorescence intensity F per unit volume can be expressed by [11]:

$$F = K.I_0.C.V.\epsilon.\Phi \tag{1}$$

with K a dimensionless factor taking account of the setup's optical transmission efficiency, I_0 the illuminating laser intensity ($W.m^{-2}$), V the illumination volume, C the fluorophore concentration ($mol.m^{-3}$), ϵ its molar absorption coefficient ($m^2.mol^{-1}$) and Φ its quantum yield (QY, unitless). In this expression K, I_0, and V depend only on power variations from the illumination system. The concentration C is mainly affected by the solvent

thermal expansion but is usually compensated via careful calibration. The molar absorption variations are assumed very small compared to the QY. The temperature impacts the fluorophore properties Φ and/or ϵ which eventually affect the emission signal. The riddance of the laser influence over fluorescence emission (often encountered with single dye laser-induced fluorescence) can be achieved by excitation of a second fluorescent dye with the same wavelength, thereby enabling fluorescence intensity normalization. In this case, the ratio R of emission signal A and B can be expressed by:

$$R = \frac{F_A}{F_B} = \frac{C_A.\epsilon_A.\Phi_A}{C_B.\epsilon_B.\Phi_B} \tag{2}$$

In addition to the illumination normalization, performing the ratio further compensates for the aforementioned solvent thermal expansion. Theoretically, volume calibration is not necessary as long as the chemical potential of both dyes is similar within the solvent. Thus two dyes LIF engineering revolves around the careful choice of dye combination to optimize thermal sensitivity.

3. Results and discussion

3.1. Fluorescence variation with temperature in bulk

Temperature influence over the emission spectra in a bi-colored solution is shown in fig. 3. The acquisition was performed by flowing a 10 μM solution of dissolved RhB and Rh110 dyes through a 100μm$\times$50μm microfluidic channel at 50 μL/h. The solvent used consists of an 80/20 mixture of water and methanol, allowing the good dissolution of both dyes while allowing future emulsification in the presence of water. Rhodamine dyes are known to have a solvent-dependent quantum yield, increasing as the solvent polarity decreases [14]. For this reason, the methanol fraction is set at 80%. The experimental setup described in fig.2 is adapted through redirection of the sample's emitted light toward a spectrometer (OCEANOPTICS USB2000+) set at 100 ms integration time. The excitation notch filter is kept before the optical fiber, and its action is visible on the emission graph.

As previously stated, the recovered signal is separated into two wavelength bands: a band <520 nm, attributed to the Rh110 signal, and a band >550nm for the RhB. Logarithmic variation of these signals confirms such attribution (increasing for Rh110 and decreasing for RhB) as well as the orders

of magnitudes measured in our system (-1.25%/°C for RhB and +0.40%/°C for Rh110).

A measurement protocol was then developed for temperature determination in solvent flowing through a microfluidic channel. Considering exponential variations of fluorescence intensity with temperature, the sensitivity coefficient s can be introduced [11]:

$$ln(\frac{R(T)}{R(T_0)}) = s(T - T_0) \tag{3}$$

with R corresponding to the ratio of fluorescence intensities originating from the two dyes $R = \frac{F_{RhB}(T)}{F_{Rh110}(T)}$. Logarithmic variation of R therefore follows a linear pattern with a slope s, T_0 being the starting temperature. The following experiments consist in establishing this parameter.

With a 50μL/h input of our dye mixture in the 100μm×50μm microfluidic channel, equipment was set back to signal acquisition by PMTs. Under these conditions, two constant signals are detected and integrated over their acquisition time (approx. 80ms). For each temperature, five measurements were acquired and averaged for each signal ('green' <520nm and 'red' >550nm), and the ratios of those averages are presented in fig.4. The presented results were normalized with the values at 20°C. The standard deviation corresponds to the average noise amplitude. The fluorescence intensity ratio decreases steadily at a -1.4%/°C linear rate. Both detection and variation showed promising results for droplet confinement.

3.2. Fluorescent droplets and variation with temperature

The same solution of 80/20 methanol/water with 10 μM Rhodamine B and Rhodamine 110 concentration is then injected into a droplet generator microfluidic chip as the dispersed phase. We proceed to emulsify the solution with a continuous phase consisting of a fluorocarbon oil mixed with a commercial surfactant for droplet stabilization (1% vol). Droplet formation is achieved by passive shearing through a nozzle of two different sizes.

Upon illumination, the fluorescence signal is acquired and analyzed with a Python script. A typical fluorescence profile acquisition is shown in fig.5. The fluorescence intensity is there taken as the area under the full width at half maximum (FWHM) of the fluorescence peaks. Upon acquisition, each peak area of the "Red" signal is integrated, then divided by its "Green" area match.

Although well detected, the validity of equation 1 is only ensured while out of saturation regime. At high laser intensity I, fluorescence emission decreases proportionally to a factor $\frac{I}{1+\frac{I}{I_{sat}}}$ with I_{sat} proper to each dye. In our experiment, control over laser power is performed via the use of a polarizer combined with a rotating analyzer (rotation difference $\Delta\alpha$). Measurement of laser power (PD-300 photo-diode OPHIR) at highest intensity ($\Delta\alpha = 0$) gives 1.6mW, which corresponds to 8kW/cm^2 considering a $\varnothing 5\mu$m Airy disk. With peak height being of great importance in droplet fluorescence determination, a saturation regime is therefore not desired in our system. The fluorescence of flowing droplets depending on the temperature and the laser intensity is presented in fig.6.

The non-linear fluorescence profile indicates dye saturation with high laser power. To avoid excessive saturation yet maintain a satisfying peak height, laser power is set at 50% of its nominal power for the rest of the experiments. Without saturation, the protocol involves 10 acquisitions of droplets' fluorescence profile, with each acquisition corresponding variation of PMT's photon count over 80ms. Depending on the droplet production rate (average 100 or 300 Hz depending on droplet size) this corresponds to an average of 10 or 25 droplets profile acquired in one measurement. An area under the curve computation grants access to droplet fluorescence required to compute the intensity ratio. Those ratios are normalized and then represented in fig.7 for 55μm droplets. A Linear regression shows -1.53%/°C variation of the fluorescence intensity ratio. This value follows the same order of magnitude as bulk flow (-1.38 and -1.44%/°C in fig.4) and the literature (-1.45%/K in [15]). The observed fluorescence ratio depends in our case on parameters seen in equation 2.

In our study, we report a diameter increase from 55μm at 20°C to 60 μm at 50°C. This volume increase therefore enhances the fluorescence signal as bigger volumes imply more fluorophores available. While this phenomenon would need to be taken into account for single-dyed droplets, the combination of 2 dyes allows us to circumvent this issue as the ratio acts also as a normalization process, allowing riddance of this size change. An increase in fluorophore amount A is thus compensated by an increase of fluorophore B (hereby Rh110 & RhB). The small variation in droplet size does not impact significantly the linear aspect of the intensity ratio considering the homogeneity of the dispersed phase.

To confront the hypothesis stated above, a similar experiment was con-

ducted with smaller droplets ($\varnothing 35\mu$m). During this experiment, the intensity ratio shows a slope of the same order of magnitude, but with a lower value (-1.41%/°C) over the 20-50°C range (fig.7).

While the fluorescence intensity variation over temperature should not depend on the droplet size or shape, a variation can still be induced by the illumination volume displacement of the system, much at stakes with smaller scales. Indeed for temperature sensing, measurements are performed with a manual displacement of the chip relative to the laser inducing a systematic error in the droplet's apex illumination. Potential radiative heating is not considered as the droplet residence time in the laser focus is short (less than 5ms). Partial illumination of the droplet leads to a weaker signal and reduced signal-to-noise ratio. Though, this variation is identical for the two dyes and can therefore also be compensated by the ratiometric computation. Still, ratiometric methods are heavily affected by uncertainty propagation and cannot compensate for low-intensity peaks and/or noisy measurements. The flaws of ratiometric measurements resides in the peak estimation algorithm. The use of lower laser power or dye concentrations would lead to a decrease of the SNR (through reducing the peak height). The peak estimation being very dependent to the noise amplitude, this would translates in estimation errors (as seen in fig.6). The 50% laser setting enables a good balance between low saturation and high SNR. In a similar manner a sufficient amount of data points per peak must be acquired for satisfying integration. This is the reason for the higher dispersion encountered with $\varnothing 35\mu$m droplets in fig.7, with less than 50 points per peak, compared to the $\varnothing 60\mu$m with up to 300 points per peak. The accuracy of this method therefore relies on peak height versus noise amplitude (SNR), as well as acquisition rate versus peak width.

3.3. Temperature measurements: cooling chip model

The method developed in this study was applied to another model system consisting of a microfluidic chip undergoing cooling in an ambient atmosphere. Soon after establishing the curve presented in fig. 7, the chip was heated up to 50°C until stationary regime ($\sim$ 5 min) and then left to cool down to room temperature set at 20°C. Measurements of fluorescence intensity shown in fig. 8 were stopped after reaching 25°C.

The incubator's in-built thermometer allows accessing the temperature of the heating plate throughout the experiment. Droplets were generated

continuously within the chip and their fluorescence profile was acquired every 30 seconds while following the previously detailed method. Considering equation 3, we compute the temperature T corresponding to each average fluorescence signal acquired during cooling using the sensitivity value previously determined in our measurements (-1.41%/°C, fig.7) and defining T_0 as the starting temperature (here 50°C, as shown in fig. 8). The uncertainty related to the computed temperature is obtained from the fluorescent signal's noise through uncertainty's propagation formulas.

Measurements from the in-built thermometer show a decreasing exponential evolution of the thermal profile over time, confirming a first-order cooling model of the system induced by natural convection. In comparison, the fluorescence ratio profile indicates an inverted trend. This inversion of the profile is expected as the dye thermal sensitivity was found negative. We proceed to the computation of the droplet temperature from the measurements of fluorescence intensity with pre-determined parameters (fig. 7). The resulting profile highlights a delayed decreasing outline, tending toward the set-point temperature curve. The shifted dynamic demonstrates the inertial effect of the material: Chip heating is performed with an external source, therefore thermalization is mainly achieved by conduction through the glass. The oil flow's low Reynolds number ($Re = 6$), i.e., a purely laminar flow, also accounts for another conductive layer. The droplet's observed temperature corresponds then to the results of the heat transfer through the glass and oil flow, delayed by the diffusive phenomenon. In this case, it is emphasized here that the two-dye LIF method application enables access to the inner temperature of droplets while flowing in the microfluidic chip. Therefore, it is demonstrated here that the chip's thermal inertia is great enough and therefore can not be neglected at the micro-metric scale for thermal dynamics study. However this result still needs to be confirmed with a more detailed study.

4. Conclusion

In this paper, we showed that fluorescence microscopy enables the high-rate assessment of temperature within micro-droplets flowing through microfluidic channels. This method, both non-intrusive and cost-effective, shows a sensitivity of -1.4%/°C in the 20-50°C range. This sensitivity was successfully demonstrated for 2 different droplet diameters obtained with various flow rates. The use of a widely available 532nm laser source, although

unconventional for this dye combination, combined with standard photo-multiplicators still allows for reasonable excitation and successful detection at a high rate. Moreover, ratio-metric computation allows compensation of illumination displacements/errors given homogeneous repartition of the two dyes within the sample. High-rate measurements could be performed and the accuracy of the method is adequate for thermal dynamic studies within droplets. This proof of concept shows the potential of two dyes LIF for the thermal study of droplets at a high rate in the micro-scale.

Notes

The authors declare no competing interests.

References

[1] M. Schulz, S. Calabrese, F. Hausladen, H. Wurm, D. Drossart, K. Stock, A. M. Sobieraj, F. Eichenseher, M. J. Loessner, M. Schmelcher, A. Gerhardts, U. Goetz, M. Handel, A. Serr, G. Haecker, J. Li, M. Specht, P. Koch, M. Meyer, P. Tepper, R. Rother, M. Jehle, S. Wadle, R. Zengerle, F. von Stetten, N. Paust, N. Borst, Point-of-care testing system for digital single cell detection of MRSA directly from nasal swabs, Lab on a Chip 20 (14) (2020) 2549–2561. doi:10.1039/D0LC00294A.

[2] N. Ghifari, B. Cinquin, A. Chahboun, A. I. El Abed, Rhodamine B Doped ZnO Monodisperse Microcapsules: Droplet-Based Synthesis, Dynamics and Self-Organization of ZnO Nanoparticles and Dye Molecules, Nanomaterials 10 (12) (2020) 2351. doi:10.3390/nano10122351.

[3] J. Teo, P. D. Pietro, F. S. Biagio, M. Capozzoli, Y.-M. Deng, I. Barr, N. Caldwell, K.-L. Ong, M. Sato, R. Tan, R. Lin, VereFlu^{TM}: An integrated multiplex RT-PCR and microarray assay for rapid detection and identification of human influenza A and B viruses using lab-on-chip technology, Archives of Virology 156 (8) (2011) 1371. doi:10.1007/s00705-011-0999-7.

[4] S. Battat, D. A. Weitz, G. M. Whitesides, An outlook on microfluidics: The promise and the challenge, Lab on a Chip 22 (3) (2022) 530–536. doi:10.1039/D1LC00731A.

[5] C. N. Baroud, F. Gallaire, R. Dangla, Dynamics of microfluidic droplets, Lab on a Chip 10 (16) (2010) 2032. doi:10.1039/c001191f.

[6] L. Shang, Y. Cheng, Y. Zhao, Emerging Droplet Microfluidics, Chemical Reviews 117 (12) (2017) 7964–8040. doi:10.1021/acs.chemrev.6b00848.

[7] J. Sakakibara, R. J. Adrian, Whole field measurement of temperature in water using two-color laser induced fluorescence, Experiments in Fluids 26 (1) (1999) 7–15. doi:10.1007/s003480050260.

[8] R. F. Kubin, A. N. Fletcher, Fluorescence quantum yields of some rhodamine dyes, Journal of Luminescence 27 (4) (1982) 455–462. doi:10.1016/0022-2313(82)90045-X.

[9] M. Snare, F. Treloar, K. Ghiggino, P. Thistlethwaite, The photophysics of rhodamine B, Journal of Photochemistry 18 (4) (1982) 335–346. doi:10.1016/0047-2670(82)87023-8.

[10] H. Rochlitz, P. Scholz, Application of laser-induced fluorescence technique in a duct flow with one heated wall, Experiments in Fluids 59 (Feb. 2018). doi:10.1007/s00348-018-2508-1.

[11] W. Chaze, O. Caballina, G. Castanet, F. Lemoine, The saturation of the fluorescence and its consequences for laser-induced fluorescence thermometry in liquid flows, Experiments in Fluids 57 (4) (2016) 58. doi:10.1007/s00348-016-2142-8.

[12] A. Abdelghany, K. Kuribayashi, M. Tange, Ratiometric laser-induced fluorescence for liquid-phase thermometry around boiling bubbles at extended temperatures above 70°c, Experiments in Fluids 63 (2) (2022) 52. doi:10.1007/s00348-022-03397-7.

[13] Z. Hayat, A. El Abed, First Experimental Evidence of Anti-Stokes Laser-Induced Fluorescence Emission in Microdroplets and Microfluidic Systems Driven by Low Thermal Conductivity of Fluorocarbon Carrier Oil, Micromachines 14 (4) (2023) 765. doi:10.3390/mi14040765.

[14] X.-F. Zhang, Y. Zhang, L. Liu, Fluorescence lifetimes and quantum yields of ten rhodamine derivatives: Structural effect on emission mechanism in different solvents, Journal of Luminescence 145 (2014) 448–453. doi:10.1016/j.jlumin.2013.07.066.

[15] V. Natrajan, K. Christensen, Development of Fluorescent Thermometry Methods for Microfluidic Systems, in: 14th Int Symp on Applications of Laser Techniques to Fluid Mechanics, 2021, p. 14.

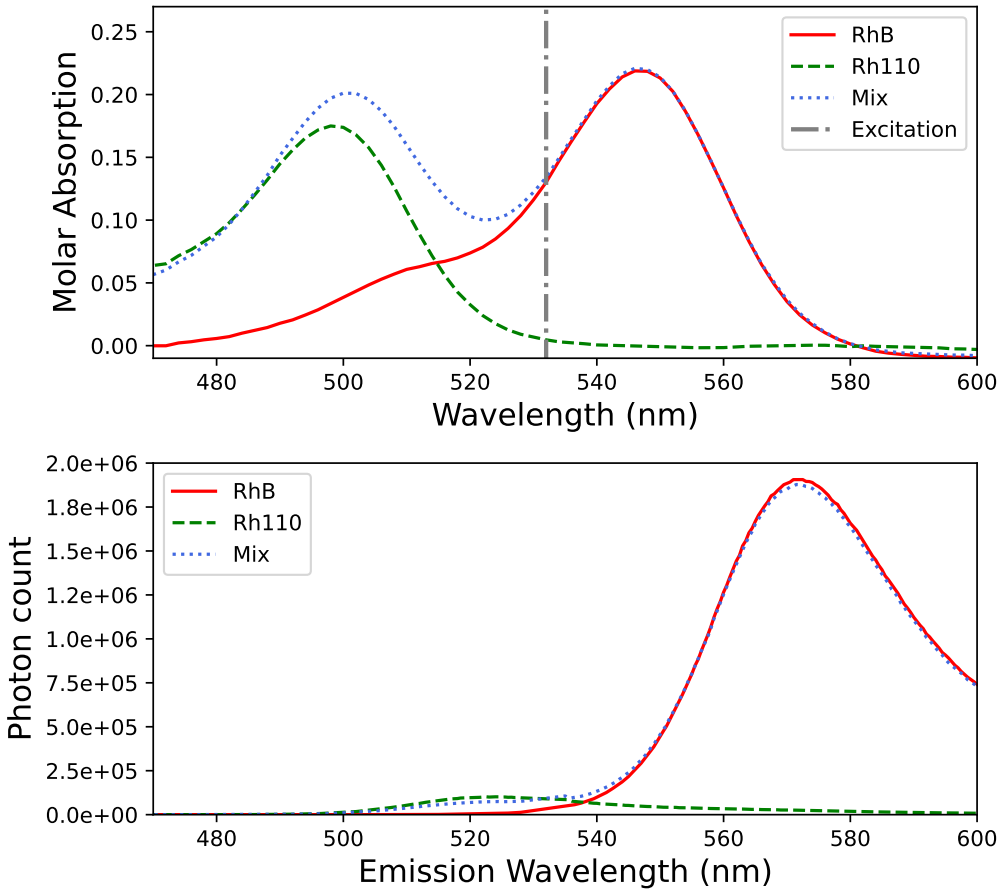

Figure 1: Up: Absorption spectra of fluorescent dyes RhB and Rh110 in methanol(80%)/water(20%), 20 °C (Spectrometer PerkinElmer Lambda 950). Bottom: Emission spectra for excitation set at 532 nm. All spectra measured in a 1 cm long quartz cuvette.

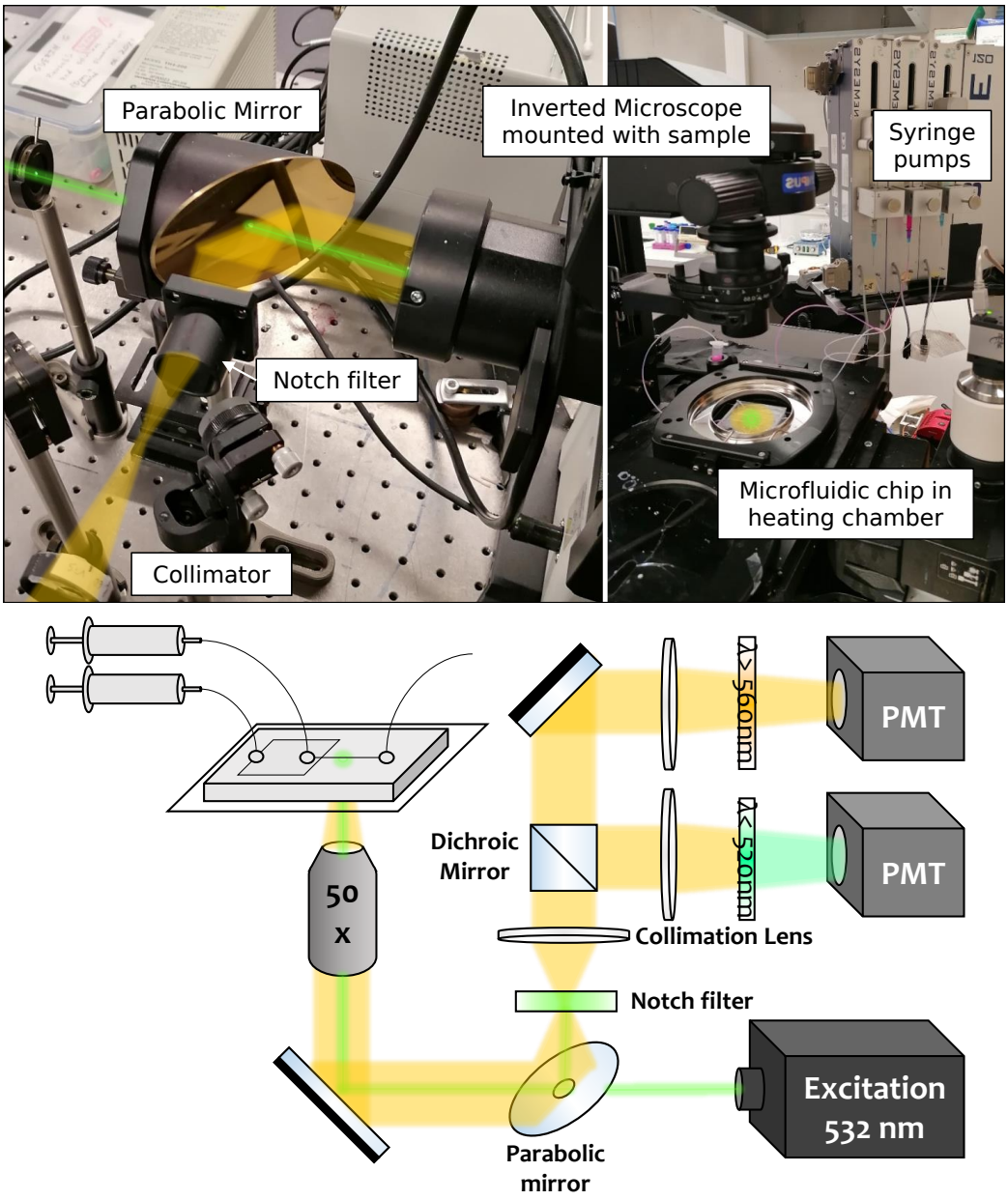

Figure 2: Experimental setup for droplet production and optical detection.

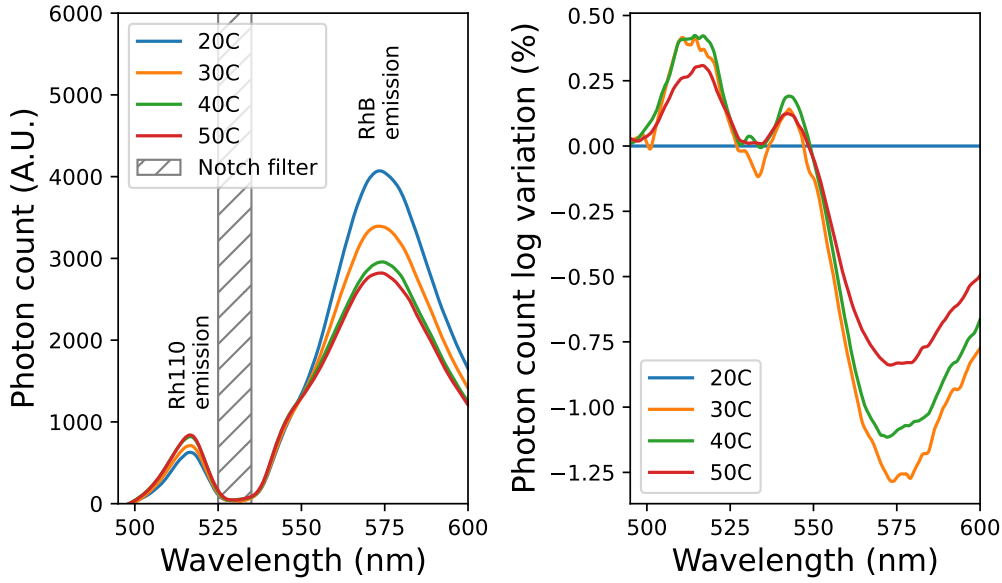

Figure 3: Left: Emission spectrum in a RhB/Rh110 mix bulk flow. Right: Photon emission Variation compared to 20°C state. A solution of methanol/water containing the 2 dyes (10 μM) is injected at 50 μL/h into a microfluidic channel (50μmx100μm section) maintained at various temperatures. Excitation 532 nm and emission signal filtered around 532 $\pm$ 5nm.

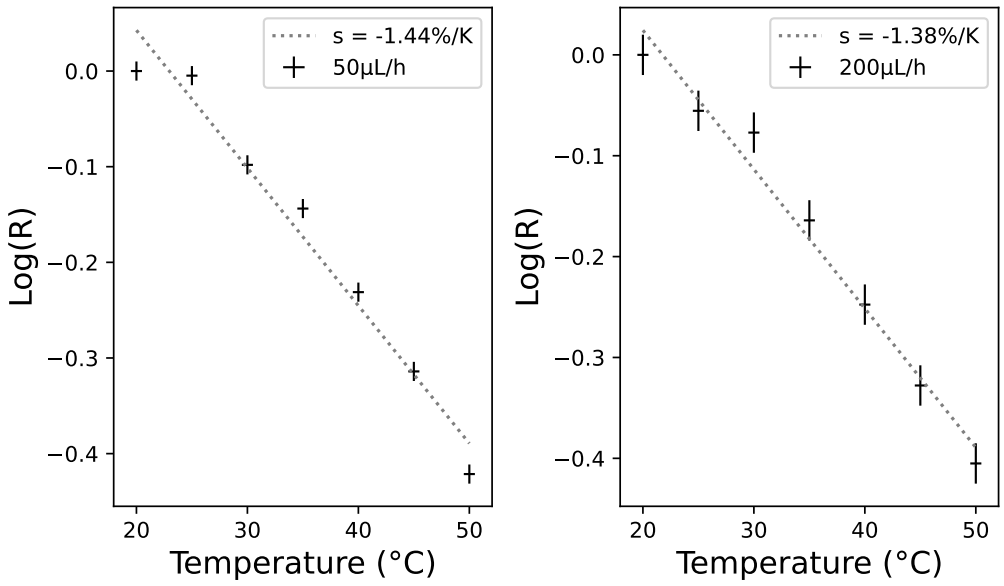

Figure 4: Fluorescence signal acquisition in bulk flow. A solution of methanol containing the 2 dyes is injected with various flow-rates (50 and 200μL/h) into a microfluidic channel (50μm×50μm section) maintained at a various temperature. The sensitivity obtained is in good agreement with literature [10][15]

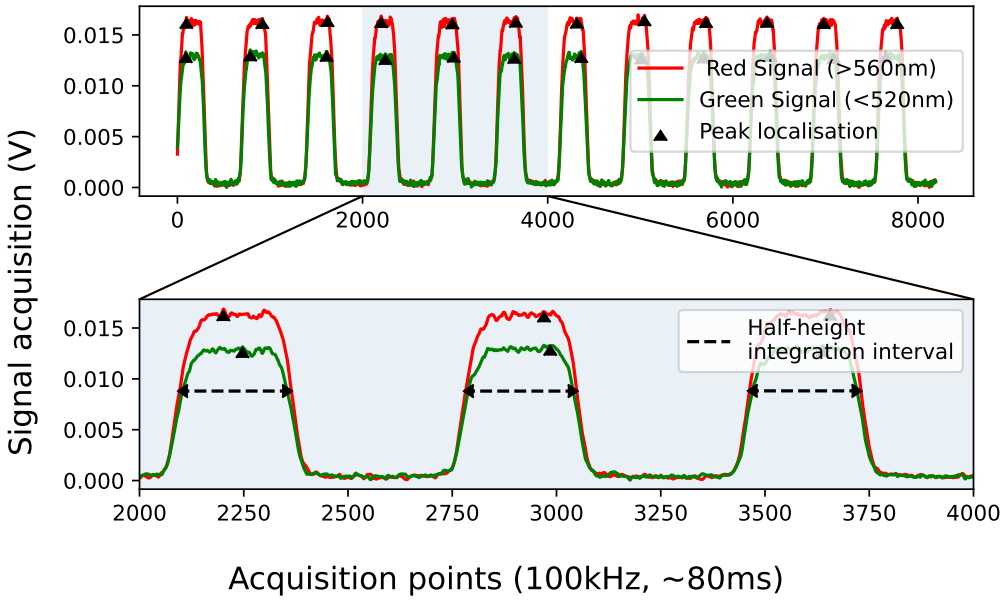

Figure 5: Fluorescence signal emitted by a train of $\varnothing 55\mu$m dyed flowing droplets at 20°C.

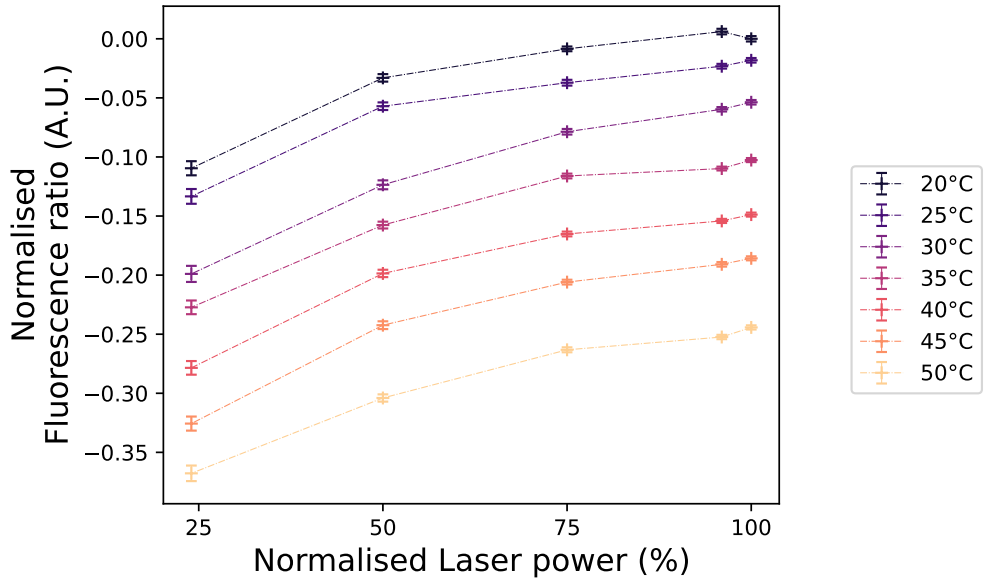

Figure 6: Representation of droplets fluorescence ratio over laser power in the [20-50]°C temperature range.

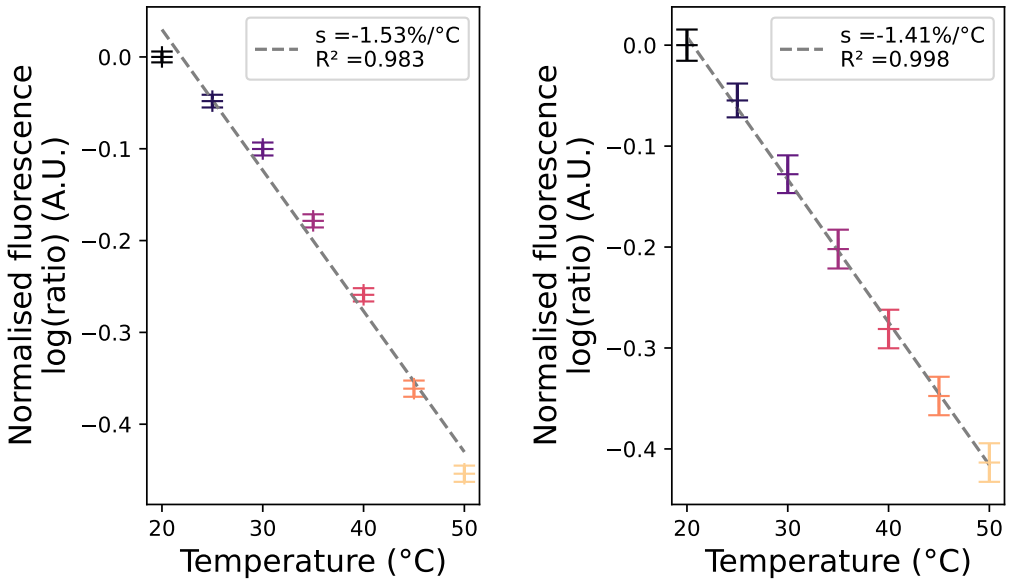

Figure 7: Fluorescence intensity ratio measurement of $\varnothing 55\mu$m droplets (left: 80 droplets/temperature sample) and $\varnothing 35\mu$m droplets (right: 250 droplets/temperature sample). Represented brackets correspond to the statistical standard deviation around the mean value.

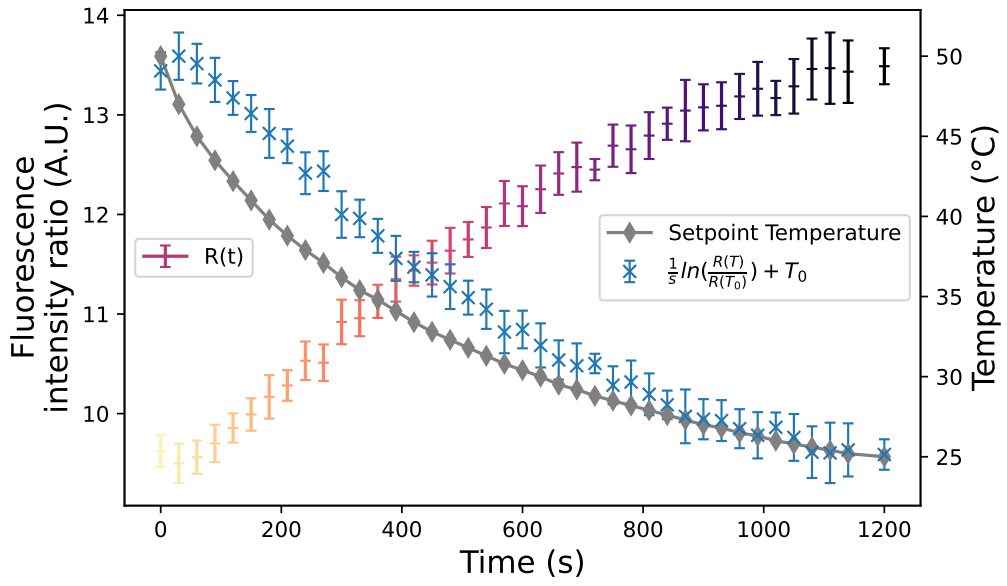

Figure 8: Fluorescence intensity ratio measurement of droplets ($\varnothing 35\mu m$) flowing through a cooling chip. Each point of $R(t)$ represents one acquisition, accounting for around 30 droplets profiles. Represented brackets correspond to the statistical standard deviation around the mean value.